JACS
JOURNAL OF THE AMERICAN CHEMICAL SOCIETY
Article
Cite This: J. Am. Chem. Soc. 2017, 139, 18552–18557
pubs.acs.org/JACS

Detection of $CO_2^{\bullet-}$ in the Electrochemical Reduction of Carbon Dioxide in *N,N*-Dimethylformamide by Scanning Electrochemical Microscopy

Tianhan Kai, Min Zhou, Zhiyao Duan, Graeme A. Henkelman, and Allen J. Bard*

Center for Electrochemistry, Department of Chemistry, The University of Texas at Austin, Austin, Texas 78712, United States

Supporting Information

ABSTRACT: The electrocatalytic reduction of CO_2 has been studied extensively and produces a number of products. The initial reaction in the CO_2 reduction is often taken to be the 1e formation of the radical anion, $CO_2^{\bullet-}$. However, the electrochemical detection and characterization of $CO_2^{\bullet-}$ is challenging because of the short lifetime of $CO_2^{\bullet-}$, which can dimerize and react with proton donors and even mild oxidants. Here, we report the generation and quantitative determination of $CO_2^{\bullet-}$ in *N,N*-dimethylformamide (DMF) with the tip generation/substrate collection (TG/SC) mode of scanning electrochemical microscopy (SECM). CO_2 was reduced at a hemisphere-shaped Hg/Pt ultramicroelectrode (UME) or a Hg/Au film UME, which were utilized as the SECM tips. The $CO_2^{\bullet-}$ produced can either dimerize to form oxalate within the nanogap between SECM tip and substrate or collected at SECM substrate (e.g., an Au UME). The collection efficiency (CE) for $CO_2^{\bullet-}$ depends on the distance (d) between the tip and substrate. The dimerization rate (6.0×10^8 M^{-1} s^{-1}) and half-life (10 ns) of $CO_2^{\bullet-}$ can be evaluated by fitting the collection efficiency vs distance curve. The dimerized species of $CO_2^{\bullet-}$, oxalate, can also be determined quantitatively. Furthermore, the formal potential ($E^{0\prime}$) and heterogeneous rate constant (k_0) for CO_2 reduction were determined with different quaternary ammonium electrolytes. The significant difference in k_0 is due to a tunneling effect caused by the adsorption of the electrolytes on the electrode surface at negative potentials.

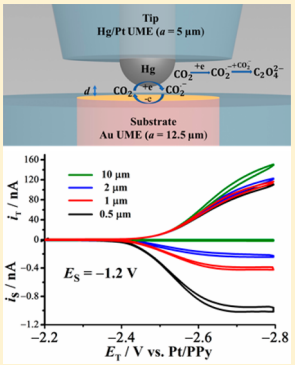

INTRODUCTION

A recent upsurge in interest in the direct and catalyzed electrochemical reduction of CO_2 stems from the possibility of converting CO_2 into fuel for energy storage and conversion.[1−3] Although extensive experimental and theoretical studies of the heterogeneous electrocatalytic (inner sphere) reactions[1,4] have been reported, the reaction mechanisms are still not clear. A generally proposed first step is the initial production of $CO_2^{\bullet-}$, through a one electron-transfer reduction at the electrode surface. The generated $CO_2^{\bullet-}$ can then be protonated, dimerize, or be further reduced to the species of interest depending on the electrode material and solution composition (reactions 1−3).[4,5]

$$CO_2 + e^- \rightleftarrows CO_2^{\bullet-} \quad (1)$$

$$CO_2^{\bullet-} + H^+ \rightarrow HCO_2^{\bullet} \quad (2)$$

$$2CO_2^{\bullet-} \rightarrow C_2O_4^{2-} \quad (3)$$

Although $CO_2^{\bullet-}$ was proposed decades ago as the initial product for CO_2 reduction, this species has rarely been observed experimentally, due to its extremely short lifetime in either aqueous or nonaqueous solutions. Since a reliable and quantitative method for its measurement has been absent, the reaction mechanism cannot be elucidated. A fair amount of effort has been spent on exploring spectroscopic methods, such as Raman[6] and Fourier transform infrared (FTIR)[7] spectroscopy, in aqueous and aprotic solutions for the detection of $CO_2^{\bullet-}$ adsorbed on the metal electrode surface. Unfortunately, quantitative information and direct electrochemical behavior of this species has not been obtained. Fast-scan cyclic voltammetry (FSCV) was used by Savéant, Amatore, and coworkers to study CO_2 reduction in anhydrous DMF.[8] The standard potential (E^0) for $CO_2/CO_2^{\bullet-}$ was evaluated to be −2.21 V vs SCE at a scan rate of 4400 V s^{-1}. The dimerization rate constant was initially calculated to be 10^7 M^{-1} s^{-1}, but this value was subsequently corrected to be 5×10^8 M^{-1} s^{-1} in their later work.[9] However, the intrinsic disadvantages of FSCV, even with ultramicroelectrodes (UMEs), such as interference by large contributions from double layer capacitance charging and adsorbed species affect the precision of the measurements, as seen in earlier experiments and make study of short-lived species difficult at high scan rates.[10] The above-mentioned problems can be circumvented by using SECM to evaluate electrochemically generated $CO_2^{\bullet-}$. Since the measurements of SECM are conducted at steady state, it has the advantage over transient electrochemical techniques in that it is not perturbed by capacitive effects and electroactive adsorbed species.[10] As a result, it is a powerful tool for the detection of extremely unstable radical species and the study of reaction mechanisms.[10] Acrylonitrile,[11] guanosine,[12] and *N,N*-dimethylani-

Received: August 15, 2017
Published: December 8, 2017

DOI: 10.1021/jacs.7b08702
J. Am. Chem. Soc. 2017, 139, 18552−18557

line[13] radicals in aprotic solution and Sn(III)[14] and superoxide[15] intermediate in aqueous solution were studied using SECM by taking advantage of the micro- or nanogap between SECM tip and substrate. Moreover, the effect of tunneling on the electron transfer rates of $Ru(bpy)_3^{2+}$ oxidation and reduction[16] and the kinetics and mechanism of radical ion annihilation mode of electrogenerated chemiluminescence (ECL)[17] were also investigated within the nanogap. Here, we propose a method to detect $CO_2^{\bullet-}$ using the TG/SC mode of SECM in DMF. Taking advantage of the nanogap and micrometer-sized electrode, we can prove the existence of $CO_2^{\bullet-}$ electrochemically at steady state. Importantly, by fitting the collection efficiency of $CO_2^{\bullet-}$ at different distances, the half-life of $CO_2^{\bullet-}$ and kinetic parameters for dimerization can be obtained. The high energetic barrier associated with a large structural change, from a linear to a V-shape as shown, for example, by DFT calculation, explains the relatively small rate of the reduction reaction. Moreover, the significant difference in the heterogeneous rate constant (k^0) for CO_2 reduction in the presence of different tetra-alkylammonium electrolytes was observed and was attributed to the effect of tunneling, through a layer of the adsorbed electrolyte at the electrode surface at relatively negative potentials. In addition, SECM can show the distribution of the products of CO_2 reduction in real-time without the need for additional analytical instruments. The obtained results indicate the possibility of utilizing SECM as an efficient tool to study the mechanism of CO_2 reduction in the presence of different homogeneous and heterogeneous catalysts.

EXPERIMENTAL SECTION

Chemicals and Materials. Mercurous nitrate ($Hg_2(NO_3)_2$; ≥ 97%), potassium nitrate (KNO_3; trace metal basis, 99%), nitric acid (HNO_3; trace metal basis), acetonitrile (CH_3CN; 99.9%), decamethylferrocene (DMFc; 99%), anhydrous *N*,*N*-dimethylformamide (DMF; 99.9%) were purchased from Fisher Scientific (Pittsburgh, PA). Tetrabutylammonium hexafluorophosphate ($TBAPF_6$; ≥99%), tetrapropylammonium hexafluorophosphate ($TPAPF_6$; ≥98%), tetraethylammonium hexafluorophosphate ($TEAPF_6$; ≥99%), tetraheptylammonium tetraphenylborate (THeATPB; selectophore), tetraoctylammonium bromide (TOABr; ≥98%), and pyrrole (99%) were acquired from Sigma-Aldrich (St. Louis, MO). All reagents were used without further purification. All aqueous solutions were prepared with ultrapure water with the resistivity of 18.3 MΩ/cm from a Milli-Q Integral system (EDM Millipore, Berllerica, MA). Argon (5.0 UHP) and carbon dioxide (10%, balance nitrogen, 4.0 UHP) gas were obtained from Praxair.

Electrode Fabrication. The process for the fabrication of disk UMEs with different radius (a) has been well described elsewhere.[10,18] In this study, we use hemisphere-shaped Hg/Pt UMEs[19,20] fabricated by electrochemical reduction of mercurous ions on a Pt UME (a = 5 μm) with RG (ratio of the radius of the electrode to that of the Pt wire) of 5. Briefly, the electrode potential was held at −100 mV vs Ag/AgCl for ∼40 s in a chronoamperometric step using an aqueous solution containing 10 mM $Hg_2(NO_3)_2$, 0.1 M KNO_3, and 0.5% HNO_3. The amount of mercury (19.0 ± 2.0 pmol) deposited on the platinum surface was deduced by integrating the chronoamperometric current, which is the total charge under the reduction peak (Figure S1). This value agrees well with the calculation (17.6 pmol) for a hemisphere. Since Pt does not dissolve appreciably in Hg, this electrode contains rather pure Hg with a very flat surface. However, the Hg/Pt UME is sensitive to vibrations and shape changes with potential at very negative values. A similar method was utilized for the fabrication of Hg/Au film UMEs.[21] In this case, a thin Hg film and essentially disk-shaped electrode is obtained, but the Hg contains appreciable Au levels. To prevent contamination from metal ions (e.g., Ag^+) and water during SECM experiments, a Pt/PPy reference electrode was fabricated by electrochemical deposition of a polypyrrole (PPy) film onto a Pt wire in CH_3CN containing 0.1 M $TBAPF_6$ and 0.01 M pyrrole as described earlier.[22] The obtained reference electrode was placed into a glass tube filled with DMF containing 0.1 M $TBAPF_6$ with a frit at one end. Good potential stability of Pt/PPy reference electrode was observed, and the potential of Pt/PPy was calibrated to be −0.19 V vs aqueous saturated calomel electrode (SCE).

Instrumentation. The electrochemical measurements were carried out with a CHI 660C potentiostat (CH Instruments, Austin, TX). A CHI 920C SECM workstation (CH Instruments, Austin, TX) for SECM measurements was placed inside an argon atmosphere drybox to avoid contamination of solution from water and oxygen. Carbon dioxide (10%) was introduced to the SECM cell directly through bubbling DMF solution for about 5 min before the experiments. The concentration of CO_2 was estimated to be 20 mM in DMF based on an earlier report.[23,24] The electrodes and cell configuration are shown in Figure 1. CO_2 was reduced on a hemisphere-shaped Hg/Pt UME (a = 5 μm), which was utilized as the SECM tip. The predominant species, oxalate, was generated by $CO_2^{\bullet-}$ dimerization at the upper portion of the hemisphere, whereas at lower portion of the hemisphere, $CO_2^{\bullet-}$ was captured by the SECM substrate (e.g., a a = 12.5 μm Au UME). A Pt/PPy electrode and a Pt wire served as the reference and counter electrodes, respectively. An accurate alignment of the SECM tip and substrate was required before the SECM experiments. The tip and substrate were initially aligned with two digital microscopes (Park, Santa Clara, CA), and then a more accurate alignment was accomplished through a x and y-axis probe scanning curve, combined with the substrate generation/tip collection (SG-TC) mode of SECM.[13] DMFc was utilized as the redox-mediator to monitor the tip position when it was in close proximity to the substrate and to determine the gap spacing (d). As indicated in Figure S2A, well-defined steady-state currents of 1 mM DMFc were obtained in anhydrous DMF containing 0.1 M $TBAPF_6$ for a a = 5 μm Hg/Pt UME and a a = 12.5 μm Au UME (Figure S2A), respectively. The steady-state current obtained agreed well with the theoretical calculation. An experimental approach curve (Figure S2B, red curve) is presented together with the theoretical COMSOL simulation (Multiphysics v4.2 software, COMSOL, Inc., Burlington, MA) within the same parameters (Figure S2B, black dotted curve). The experimental results are well in line with the simulated result, which also indicates the accurate alignment of the tip and substrate.

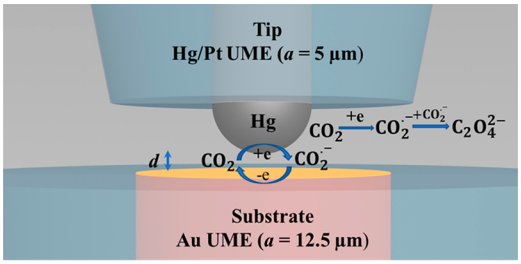

Figure 1. Schematic depiction of the collection of the $CO_2^{\bullet-}$ radical in TG/SC mode of SECM.

DFT Simulation. The spin-polarized density functional theory (DFT) calculations were performed using the projector-augmented wave (PAW) method[25] as implemented in the Vienna ab initio simulation package (VASP).[26] An energy cutoff of 600 eV for the plane wave basis set was used to expand the Kohn−Sham orbitals. The hybrid density functional theory proposed by Heyd, Scuseria, and Ernzerhof (HSE06)[27] was used to approximate the electronic exchange and correlation. Solvation effects, which are prominent in stabilizing ionic species, were taken into account by using an implicit solvation model implemented into VASP by Mathew and Hennig.[28] The background dielectric constant of DMF was set to 36.7.

DOI: 10.1021/jacs.7b08702
J. Am. Chem. Soc. 2017, 139, 18552−18557

RESULTS AND DISCUSSION

CV of CO_2 Reduction. Cyclic voltammogram (CV) of 20 mM CO_2 at a Hg/Pt UME (a = 5 μm) in DMF containing 0.1 M $TBAPF_6$ is shown in Figure 2. Well-defined reduction waves

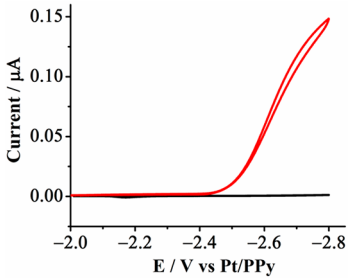

Figure 2. CVs of a Hg/Pt UME (a = 5 μm) in DMF containing 0.1 M $TBAPF_6$ in the absence (black curve) and presence of 20 mM CO_2 (red curve) at a scan rate of 100 mV s^{-1}.

(red curve) were observed with the half-wave potential ($E_{1/2}$) of −2.63 V. The steady-state current (i_{ss}), 0.15 μA, was obtained. The number of the electrons transferred (n = 0.92) was deduced using eq 4

$$i_{ss} = 2\pi nFDca \quad (4)$$

where F is the Faraday constant (96 500 C mol^{-1}), D is the diffusion coefficient (2.7 × 10^{-5} cm^2 s^{-1}),[9] c is the concentration of CO_2 (20 mM), and a is the radius of the UME (5 μm). The background current was negligible in the absence of CO_2 (black curve). Pt can be easily wet by Hg and yet has a low solubility in it, and the identical CO_2 reduction waves were obtained repeatedly at the Hg/Pt UMEs. No adsorption of CO_2 and/or of its reduction intermediates (e.g., $CO_2^{\bullet-}$) was apparent, thus Hg can be considered as a suitable electrochemical material for CO_2 reduction.[5,9] Although the results indicate that the reduction process at the Hg/Pt surface consumes one electron per mole of CO_2, the lack of a current plateau was observed and was mainly attributed to the instability of the Hg/Pt UME at the very negative potentials.

CO_2 Reduction by TG/SC Mode of SECM. TG/SC mode of SECM was employed for the studies of CO_2 reduction. Since the $CO_2^{\bullet-}$ does not adsorb on the Hg/Pt surface, once it is generated at the SECM tip (a a = 5 μm Hg/Pt UME), it diffuses away and is collected by an SECM substrate (e.g., a a = 12.5 μm Au UME). To accomplish that, a small d (distance between tip and substrate) is required, so that $CO_2^{\bullet-}$ can diffuse across the gap before further reactions take place. In order to assess the redox behavior of $CO_2^{\bullet-}$, the tip potential (E_T) was held constant at −2.8 V to generate $CO_2^{\bullet-}$ continuously (Figure 3A, red curve), whereas the substrate potential (E_S) was scanned from −2.1 V to −0.9 V to collect the generated $CO_2^{\bullet-}$. The collection of $CO_2^{\bullet-}$ (Figure 3A, black curve) is shown by the increase of substrate current (i_S) at d of 1 μm. The tip current (i_T) increased under this condition because some $CO_2^{\bullet-}$ was oxidized back to CO_2 at the substrate and fed back to the tip. Since i_T reached a plateau at around −1.2 V, E_S was held at −1.2 V in Figure 3B to collect the generated $CO_2^{\bullet-}$ at different d to evaluate the variation of i_S with d. The reduction of 20 mM CO_2 at the SECM tip was conducted (Figure 3B, top) by sweeping E_T from −2.2 V to −2.8 V, while E_S was held constant at −1.2 V to oxidize $CO_2^{\bullet-}$ back to CO_2 (Figure 3B, bottom). As d decreased from 10 μm

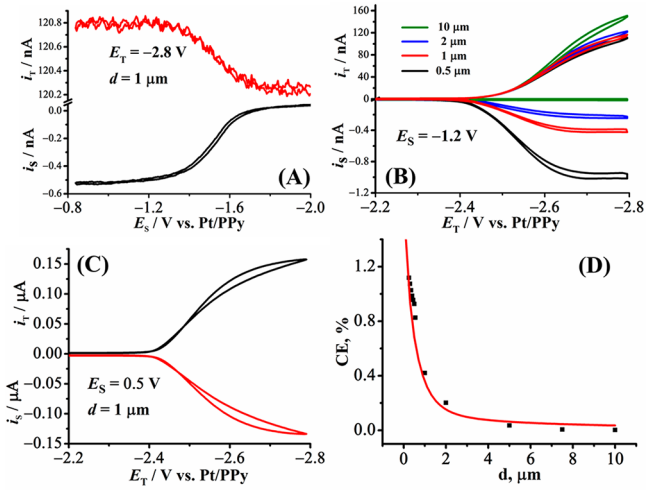

Figure 3. (A) $CO_2^{\bullet-}$ (black curve) collected at a SECM substrate (a a = 12.5 μm Au UME) in DMF containing 0.1 M $TBAPF_6$ by holding E_T at −2.8 V, while scanning E_S from −2.1 V to −0.9 V (d = 1 μm). i_T is shown in the red curve. (B) CVs of 20 mM CO_2 reduction (top) acquired at a SECM tip (a a = 5 μm Hg/Pt UME) and corresponding i_S of $CO_2^{\bullet-}$ (bottom) at the d of 10 (green), 2 (blue), 1 (red), and 0.5 μm (black curve), respectively. The E_S was held at −1.2 V while scanning E_T from −2.2 V to −2.8 V. Part C is the same as part B except the E_S was held at 0.5 V to collect oxalate (red curve) at d of 1 μm. (D) Experimental CE (black dotted) of $CO_2^{\bullet-}$ and the best fit of the results (red curve) with the EC model of simulation. The scan rates for parts A−C were 100 mV/s.

to 200 nm, i_T decreased because of the hindered diffusion. Meanwhile, i_S was only observable when the tip was close to the substrate ($d \leq 2$ μm) and increased with smaller d. The dimerized species of $CO_2^{\bullet-}$, oxalate, can also be captured at the substrate by holding E_S at a more positive potential, 0.5 V (Figure 3C, red curve), while sweeping the E_T from −2.2 V to −2.8 V (Figure 3C, black curve). For the determination of oxalate, the solution in SECM needed to be replaced by fresh electrolyte without DMFc to prevent interference by its oxidation. The high CE (~90%, d = 1 μm) for oxalate indicates that it is the predominant species during the CO_2 reduction at Hg/Pt UMEs. Although $CO_2^{\bullet-}$ can react with CO_2 or trace amounts of water based on the previous report,[5] the dimerization clearly predominates over other reactions under our experimental conditions. This observation is consistent with another report by Savéant and co-workers.[9] The CE for $CO_2^{\bullet-}$ is small, even at small d, as shown in Figure 3D (black dotted curve). As d decreased from 10 μm to 200 nm, the CE increased to 1.1%. The relatively low CE was primarily due to the extremely fast dimerization rate of $CO_2^{\bullet-}$; the hemispherical shape of the SECM tip (Figure 1) also contributes. We calculated the dimerization rate of $CO_2^{\bullet-}$ using COMSOL Multiphysics v4.2 software as described in Figure S3. The best fit of the CE curve as a function of d, with the EC model for a given rate constant (k_c) for the dimerization reaction, is shown in Figure 3D (red curve). Comparing the simulated and experimental data indicated that k_c is about 6.0 × 10^8 M^{-1} s^{-1}. The half-life of $CO_2^{\bullet-}$, $t_{1/2}$, is about 10 ns using the equation of $t_{1/2} = 1/(k_c c)$. These values represent the fastest homogeneous coupling reaction and shortest half-life measured electrochemically to date.

To alleviate possible problems with a hemispherical Hg/Pt UME, experiments were also carried out with a Hg/Au

DOI: 10.1021/jacs.7b08702
J. Am. Chem. Soc. 2017, 139, 18552−18557

electrode with a thin Hg film on an Au UME. Results for this electrode for CO_2 reduction are shown in Figure 4. In general,

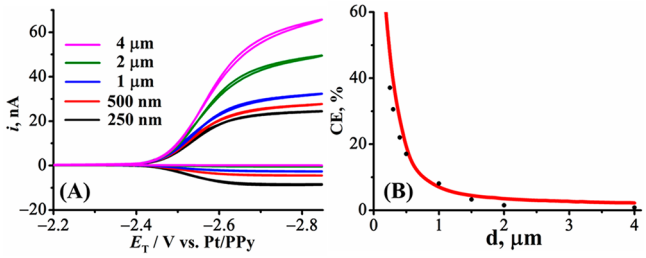

Figure 4. (A) 20 mM CO_2 reduction (top) at a SECM tip (a a = 5 μm Hg/Au UME) and corresponding collection currents of $CO_2^{\bullet-}$ (bottom) at a SECM substrate (a a = 12.5 μm Au UME) in DMF containing 0.1 M $TBAPF_6$ at different d values (4, 2, 1, 0.5, and 0.25 μm). The E_S was held at −1.2 V while scanning E_T from −2.2 V to −2.85 V. (B) Experimental CE (black dotted) and the best fit of the experimental data (red curve) for $CO_2^{\bullet-}$ with the EC model of simulation.

the results are similar to those with the Hg/Pt UME, but higher collection efficiencies (~37%) and more resolved limiting currents were found. UMEs with other metals (Pt and Au) were also tried as tips for the reduction of CO_2 in DMF. However, satisfactory and repeatable CVs could not be obtained.

The electrochemical behavior of $CO_2^{\bullet-}$ was also evaluated with different SECM substrate collectors (Pt and Hg/Au) using a Hg/Pt UME as the tip (Figure S4). A shift of $CO_2^{\bullet-}$ oxidation in the positive direction at a Pt substrate was observed (Figure S4, red curve). This might be caused by the passivation of the Pt surface by trace amounts of CO in the solution.[29]

Heterogeneous Electron Transfer (ET) Rate of CO_2 Reduction. In general, the rates of simple 1e transfer are quite large. Under these conditions, the radical ion produced can be detected[11−13] using the TG/SC mode of SECM by holding E_S close to the onset potential of the reduction at the tip. However, for the CO_2 reduction, a large separation of potential for reduction ($E_{1/2}$= −2.63 V, Figure 2) and product oxidation ($E_{1/2}$= −1.51 V, Figure 3) is found, indicating a slower ET reaction. This can be attributed to the large reorganization energy, i.e., the Marcus λ_I, because of a large structural change on ET. It is well-known that CO_2 undergoes a large structural change, from a linear to a V-shape on reduction. To address this, DFT calculations were employed to estimate the magnitude of the inner and outer reorganization energy of the reaction. After the structure of CO_2 and $CO_2^{\bullet-}$ was optimized, we obtained the potential energy curves (PECs) for CO_2 + e (Figure S5A, blue curve) and $CO_2^{\bullet-}$ (Figure S5A, red curve), which were evaluated as a function of reaction coordinate (bent angle 180−135° and C−O bond length 1.162−1.234 Å) under implicit solvent (DMF) with a dielectric constant of 36.7. The energy surface for CO_2 follows a parabolic shape. $CO_2^{\bullet-}$ remains stable when the molecule is bent. In the absence of solvent and electrolyte, once $CO_2^{\bullet-}$ is halfway from the bent to the linear structure, $CO_2^{\bullet-}$ is no longer stable due to the facile detachment of an electron from the $CO_2^{\bullet-}$ molecule. Note that the loss of an electron from $CO_2^{\bullet-}$ could be an artifact due to the missing cation in our simulation. At the predicted equilibrium potential (E_{eq} = −2.4 V vs SHE), the Gibbs activation energy (ΔG^*) for CO_2 reduction is calculated to be 0.5 eV (Figure S5B). On the basis of the simulation, k^0 is estimated to be 2.2 × 10^{-4} cm s^{-1} using eq 5[18,30]

$$k^0 = K_p \nu_n k \exp\left(-\frac{\Delta G^*}{RT}\right) \quad (5)$$

where κ is the electronic transmission coefficient, which is taken initially as unity, assuming that CO_2 reduction at the Hg/Pt surface is a purely adiabatic reaction (Figure 2); K_p is the precursor equilibrium constant (~60 pm);[30] and ν_n is the nuclear frequency factor (1.1 × 10^{12} s^{-1}), which was determined by eq 6[30]

$$\nu_n = \tau_L^{-1}\left(\frac{\Delta G^*}{4\pi RT}\right)^{1/2} \quad (6)$$

where $\tau_L$is the longitudinal solvent relaxation time (1.1 ps for DMF).[31] The estimated k^0 represents an upper limit of the reaction rate. The uncertainty of the theoretically estimated k^0 largely relies on the uncertainty of the value of κ, which is determined by the adiabaticity of the reaction.

Effect of Tunneling on the ET Rate. There has been recent interest in the effects of tunneling on electrode reactions.[32−36] Since κ exponentially depends on the distance between the electrode and reactant, we carried out CV experiments with electrolytes of different sizes, so that the nature of the reaction can be determined from the behavior of k^0 as a function of electrolyte size. The CVs of CO_2 reduction on a Hg/Pt UME (a = 5 μm) containing different electrolytes are shown in Figure 5. The $E_{1/2}$ shifted the negative direction

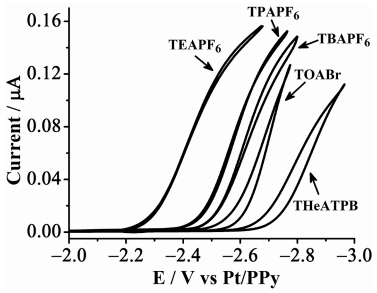

Figure 5. CVs of 20 mM CO_2 reduction collected at a Hg/Pt UME (a = 5 μm) in DMF solution containing 0.1 M $TEAPF_6$, $TPAPF_6$, $TBAPF_6$, THeATPB, and TOABr, respectively.

from −2.38 V ($TEAPF_6$) to −2.67 V (TOABr) with the increase of cation size, except for THeATPB, which shows the most negative reduction potential ($E_{1/2}$ = −2.83 V). Fawcett[37] and Evans[38] and co-workers attributed this phenomenon to a tunneling effect which occurs for reduction at relatively negative potential with respect to the potential of zero charge (PZC). The negatively charged electrode adsorbs a large amount of cations, which subsequently form a dense layer on the electrode, preventing the close approach of CO_2 to the electrode surface and further slows the electron transfer. On the basis of our results, the size of the anion of the supporting electrolyte may also contribute to the thickness of the tunneling layer. Capacitance measurements in the presence of different electrolytes at relatively negative potentials were conducted and the total double layer capacitance was calculated, as shown in Table S1. The double layer capacitance decreases as the size of the electrolytes increase, indicating the existence of an adsorbed electrolyte species on the electrode surface.[37]

DOI: 10.1021/jacs.7b08702
J. Am. Chem. Soc. 2017, 139, 18552−18557

Table 1. Potentials and Kinetic Parameters[a] for 20 mM CO_2 Reduction from Steady-State Voltammograms Using 0.1 M $TEAPF_6$ and $TBAPF_6$, Respectively

	electrolyte	$E_{1/2}{}^{c}$ (V)	$E_{1/2}{}^{a}$ (V)	$E^{0\prime}$ (V)	D,[b] cm^2/s	α	k_c, M^{-1} s^{-1}	k^0, cm/s
Hg/Pt UME	0.1 M $TEAPF_6$	−2.57	−1.91	−2.24	2.3×10^{-5}	0.42	6.0×10^{8}	1.5×10^{-4}
Hg/Pt UME	0.1 M $TBAPF_6$	−2.82	−1.70	−2.26	2.3×10^{-5}	0.45	6.0×10^{8}	2.4×10^{-6}
Hg/Au UME	0.1 M $TBAPF_6$			−2.26	2.3×10^{-5}	0.56	6.0×10^{8}	1.0×10^{-6}

[a]The potential was converted to values vs aqueous SCE. [b]D was corrected to be 2.3×10^{-5} cm^2/s for the best fit.

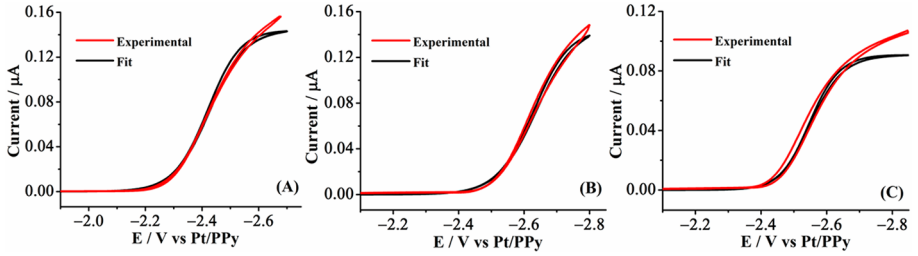

Figure 6. Experimental (red) and simulated CVs (black curves) for 20 mM CO_2 reduction at a Hg/Pt UME (a = 5 μm, A and B) and a Hg/Au UME (a = 5 μm, C) in the presence of 0.1 M $TEAPF_6$ (A) and 0.1 M $TBAPF_6$ (B and C), respectively. The parameters are shown in Table 1.

An alternative explanation of supporting electrolyte effects involves ion pairing of the cation with $CO_2^{\bullet-}$. We can test this by examining whether the formal potential for CO_2 reduction ($E^{0\prime}$), estimated as the average of the cathodic and anodic $E_{1/2}$ values, e.g., for $TEAPF_6$ and $TBAPF_6$, are the same. Significant ion paring should assist in the formation of $CO_2^{\bullet-}$ and cause a positive shift in potential. In order to assess that, the voltammetric behavior of $CO_2^{\bullet-}$ at a Hg/Au UME (a = 12.5 μm) was obtained in Figure S6. As shown in Table 1, $E^{0\prime}$ for the TEA^+ and TBA^+ salts are −2.24 and −2.26 V, respectively, suggesting lack of ion pairing.

We obtained k^0 for 20 mM CO_2 reduction at a a = 5 μm Hg/Pt UME by simulating the experimental voltammograms with 0.1 M $TEAPF_6$ (Figure 6A) and 0.1 M $TBAPF_6$ solution (Figure 6B), respectively, using Digielch software (Gamry Inc., Warminster, PA). The simulation included the effect of the dimerization reaction. The results are shown in Table 1. The larger k^0 of the $TEAPF_6$ solution is also consistent with the tunneling model. The simulation of the experimental voltammogram of 20 mM CO_2 reduction at a a = 5 μm Hg/Au UME with 0.1 M $TBAPF_6$ was also conducted, as shown in Figure 6C. The value of k^0 (1.0×10^{-6} cm/s) was comparable with the one obtained at the Hg/Pt UME in 0.1 M $TBAPF_6$ (3.0×10^{-6} cm/s). However, the changes in the shape of the Hg hemisphere and side reactions at steady-state region affect the accurate measurements of k^0. This part will be improved and kinetics studies of the side reactions will also be conducted in planned new studies.

CONCLUSIONS

SECM was utilized to study the mechanism of CO_2 reduction. The initial product, an unstable intermediate, $CO_2^{\bullet-}$, was captured for the first time using the TG/SC mode of SECM. We were able to accurately assess the dimerization rate (6.0×10^8 M^{-1} s^{-1}) and half-life (10 ns) of $CO_2^{\bullet-}$ by fitting the experimental data with the theoretical simulation. This represents the fastest homogeneous coupling reaction and shortest half-life that has been measured electrochemically. Our experimental data and DFT calculation both verified the irreversibility of the reaction. Formal potential ($E^{0\prime}$) and heterogeneous rate constant (k_0) for CO_2 reduction were calculated with $TEAPF_6$ and $TBAPF_6$ as electrolytes, respectively. The significant difference in k_0 is due to the "tunneling effect" caused by the adsorption of the electrolyte on the electrode surface at negative potential with respect to PZC. Moreover, the capability of quantitative and real-time detection of stable products (e.g., oxalate) during CO_2 reduction also facilitates the analysis of the product distribution of CO_2 reduction. To the best of our knowledge, this is the first report to present a way to quantitatively measure $CO_2^{\bullet-}$ in aprotic solution without the interference of capacitive charging. As $CO_2^{\bullet-}$ is a critical species during CO_2 reduction, the ability to quantitatively measure this intermediate within the nanogap provides the possibility of utilizing SECM as a tool to conduct mechanism studies for CO_2 reduction with heterogeneous and homogeneous catalysts.

ASSOCIATED CONTENT

Supporting Information

The Supporting Information is available free of charge on the ACS Publications website at DOI: 10.1021/jacs.7b08702.

Chronoamperogram of mercury deposition at a Pt UME;, CV and approach curve of UMEs, COMSOL simulation parameters, CV of $CO_2^{\bullet-}$ at different substrates, DFT calculation, capacities calculation, and collection of $CO_2^{\bullet-}$ with $TEAPF_6$ as an electrolyte (PDF)

AUTHOR INFORMATION

Corresponding Author

*ajbard@mail.utexas.edu

ORCID

Tianhan Kai: 0000-0001-5667-1426

Graeme A. Henkelman: 0000-0002-0336-7153

Allen J. Bard: 0000-0002-8517-0230

Notes

The authors declare no competing financial interest.

ACKNOWLEDGMENTS

We acknowledge the support of this research from the AFOSR MURI (Grant FA9550-14-1-0003) and Robert A. Welch Foundation (Grants F-0021 and F-1841).

DOI: 10.1021/jacs.7b08702
J. Am. Chem. Soc. 2017, 139, 18552−18557

REFERENCES

(1) Hori, Y. Electrochemical CO_2 reduction on metal electrodes. In *Modern Aspects of Electrochemistry*; Vayenas, C., White, R., Gamboa-Aldeco, M., Eds.; Springer: New York, 2008; Vol. *42*, p 89.
(2) Kim, D.; Sakimoto, K. K.; Hong, D. C.; Yang, P. D. *Angew. Chem., Int. Ed.* **2015**, *54*, 3259.
(3) Olah, G. A.; Prakash, G. S.; Goeppert, A. *J. Am. Chem. Soc.* **2011**, *133*, 12881.
(4) Costentin, C.; Robert, M.; Saveant, J. M. *Chem. Soc. Rev.* **2013**, *42*, 2423.
(5) Amatore, C.; Saveant, J. M. *J. Am. Chem. Soc.* **1981**, *103*, 5021.
(6) Mcquillan, A. J.; Hendra, P. J.; Fleischmann, M. *J. Electroanal. Chem. Interfacial Electrochem.* **1975**, *65*, 933.
(7) Chandrasekaran, K.; Bockris, J. O. *Surf. Sci.* **1987**, *185*, 495.
(8) Lamy, E.; Nadjo, L.; Saveant, J. M. *J. Electroanal. Chem. Interfacial Electrochem.* **1977**, *78*, 403.
(9) Gennaro, A.; Isse, A. A.; Severin, M. G.; Vianello, E.; Bhugun, I.; Saveant, J. M. *J. Chem. Soc., Faraday Trans.* **1996**, *92*, 3963.
(10) Bard, A. J.; Mirkin, M. V. *Scanning Electrochemical Microscopy*, 2nd ed.; CRC Press: Boca Raton, FL, 2012.
(11) Zhou, F. M.; Bard, A. J. *J. Am. Chem. Soc.* **1994**, *116*, 393.
(12) Bi, S. P.; Liu, B.; Fan, F. R. F.; Bard, A. J. *J. Am. Chem. Soc.* **2005**, *127*, 3690.
(13) Cao, F. H.; Kim, J.; Bard, A. J. *J. Am. Chem. Soc.* **2014**, *136*, 18163.
(14) Chang, J. H.; Bard, A. J. *J. Am. Chem. Soc.* **2014**, *136*, 311.
(15) Zhou, M.; Yu, Y.; Hu, K. K.; Mirkin, M. V. *J. Am. Chem. Soc.* **2015**, *137*, 6517.
(16) Shen, M.; Bard, A. J. *J. Am. Chem. Soc.* **2011**, *133*, 15737.
(17) Rodríguez-López, J.; Shen, M.; Nepomnyashchii, A. B.; Bard, A. J. *J. Am. Chem. Soc.* **2012**, *134*, 9240.
(18) Bard, A. J.; Faulkner, L. R. *Electrochemical Methods: Fundamentals and Applications*, 2nd ed.; John Wiley & Sons: New York, 2001.
(19) Mauzeroll, J.; Hueske, E. A.; Bard, A. J. *Anal. Chem.* **2003**, *75*, 3880.
(20) Wehmeyer, K. R.; Wightman, R. M. *Anal. Chem.* **1985**, *57*, 1989.
(21) Jung, C. H.; Sanchez-Sanchez, C. M.; Lin, C. L.; Rodriguez-Lopez, J.; Bard, A. J. *Anal. Chem.* **2009**, *81*, 7003.
(22) Ghilane, J.; Hapiot, P.; Bard, A. J. *Anal. Chem.* **2006**, *78*, 6868.
(23) Gennaro, A.; Isse, A. A.; Vianello, E. *J. Electroanal. Chem. Interfacial Electrochem.* **1990**, *289*, 203.
(24) Wadhawan, J. D.; Welford, P. J.; McPeak, H. B.; Hahn, C. E. W.; Compton, R. G. *Sens. Actuators, B* **2003**, *88*, 40.
(25) Kresse, G.; Hafner, J. *Phys. Rev. B: Condens. Matter Mater. Phys.* **1993**, *47*, 558.
(26) Kresse, G.; Joubert, D. *Phys. Rev. B: Condens. Matter Mater. Phys.* **1999**, *59*, 1758.
(27) Heyd, J.; Scuseria, G. E.; Ernzerhof, M. *J. Chem. Phys.* **2003**, *118*, 8207.
(28) Fishman, M.; Zhuang, H. L.; Mathew, K.; Dirschka, W.; Hennig, R. G. *Phys. Rev. B: Condens. Matter Mater. Phys.* **2013**, *87*, 245402.
(29) Dhar, K.; Cavallotti, C. *J. Phys. Chem. A* **2014**, *118*, 8676.
(30) Fawcett, W. R.; Opallo, M. *Angew. Chem., Int. Ed. Engl.* **1994**, *33*, 2131.
(31) Fawcett, W. R.; Foss, C. A. *Electrochim. Acta* **1991**, *36*, 1767.
(32) Barfidokht, A.; Ciampi, S.; Luais, E.; Darwish, N.; Gooding, J. J. *Anal. Chem.* **2013**, *85*, 1073.
(33) Chazalviel, J. N.; Allongue, P. *J. Am. Chem. Soc.* **2011**, *133*, 762.
(34) Gosavi, S.; Marcus, R. A. *J. Phys. Chem. B* **2000**, *104*, 2067.
(35) Hill, C. M.; Kim, J.; Bard, A. J. *J. Am. Chem. Soc.* **2015**, *137*, 11321.
(36) Hill, C. M.; Kim, J.; Bodappa, N.; Bard, A. J. *J. Am. Chem. Soc.* **2017**, *139*, 6114.
(37) Fawcett, W. R.; Fedurco, M.; Opallo, M. *J. Phys. Chem.* **1992**, *96*, 9959.
(38) Evans, D. H. *Chem. Rev.* **2008**, *108*, 2113.

DOI: 10.1021/jacs.7b08702
J. Am. Chem. Soc. 2017, 139, 18552−18557